Article

Folding and Lipid Composition Determine Membrane Interaction of the Disordered Protein COR15A

Carlos Navarro-Retamal,[1] Anne Bremer,[2] Helgi I. Ingólfsson,[3] Jans Alzate-Morales,[1] Julio Caballero,[1] Anja Thalhammer,[4] Wendy González,[1,5] and Dirk K. Hincha[2,*]

[1]Center for Bioinformatics and Molecular Simulations, Universidad de Talca, Casilla, Talca, Chile; [2]Max-Planck-Institut für Molekulare Pflanzenphysiologie, Potsdam, Germany; [3]Groningen Biomolecular Sciences and Biotechnology Institute and Zernike Institute for Advanced Materials, University of Groningen, AG Groningen, The Netherlands; [4]Physikalische Biochemie, Universität Potsdam, Potsdam, Germany; and [5]Millennium Nucleus of Ion Channels-Associated Diseases (MiNICAD), Universidad de Talca, Casilla, Talca, Chile

ABSTRACT   Plants from temperate climates, such as the model plant *Arabidopsis thaliana*, are challenged with seasonal low temperatures that lead to increased freezing tolerance in fall in a process termed cold acclimation. Among other adaptations, this involves the accumulation of cold-regulated (COR) proteins, such as the intrinsically disordered chloroplast-localized protein COR15A. Together with its close homolog COR15B, it stabilizes chloroplast membranes during freezing. COR15A folds into amphipathic α-helices in the presence of high concentrations of low-molecular-mass crowders or upon dehydration. Under these conditions, the (partially) folded protein binds peripherally to membranes. In our study, we have used coarse-grained molecular dynamics simulations to elucidate the details of COR15A-membrane binding and its effects on membrane structure and dynamics. Simulation results indicate that at least partial folding of COR15A and the presence of highly unsaturated galactolipids in the membranes are necessary for efficient membrane binding. The bound protein is stabilized on the membrane by interactions of charged and polar amino acids with galactolipid headgroups and by interactions of hydrophobic amino acids with the upper part of the fatty acyl chains. Experimentally, the presence of liposomes made from a mixture of lipids mimicking chloroplast membranes induces additional folding in COR15A under conditions of partial dehydration, in agreement with the simulation results.

INTRODUCTION

Plants are constantly exposed to a wide range of abiotic stresses, such as drought, salinity, and high and low temperatures. Plants native to temperate and boreal climates are challenged with seasonal low temperatures that may result in freezing stress, i.e., the crystallization of ice in the intercellular spaces, in particular in the exposed above-ground tissues. Such plant species are able to increase their freezing tolerance in fall in response to low temperatures above the freezing point in a process termed cold acclimation (1–3). In the model plant *Arabidopsis thaliana*, massive changes in gene expression occur during cold acclimation, leading, among other reactions, to the accumulation of cold-regu-

lated (COR) proteins (4). Although the physiological function of most of these proteins is still unknown, the two chloroplast-localized proteins COR15A and COR15B function redundantly in the stabilization of chloroplast membranes during the freezing of leaves (5).

COR15A/B and several other COR proteins belong to the larger group of late embryogenesis abundant (LEA) proteins. There are 51 genes in the *Arabidopsis* genome that encode LEA proteins. They are divided into nine families based on amino acid sequence domains, and COR15A and B belong to the Pfam LEA_4 (PF02987) family that consists of 18 members (6). Members of this protein family have also been identified in other plant species and several species of invertebrate animals (7,8). All LEA_4 proteins that have been characterized so far are intrinsically disordered proteins (IDP) that show no stable secondary structure in dilute solutions. However, several LEA_4 proteins form amphipathic α-helices during drying (see (7,9) for reviews).

Folding of the COR15 proteins can also be induced by trifluoroethanol and glycerol (5,10). Molecular dynamics (MD) simulations indicate that glycerol stabilizes the folded state because it is excluded from the proteins leading to backbone dehydration (11), as suggested previously for the folding of IDPs in the presence of other osmolytes (12–14). Additional folding is induced in COR15 proteins suspended in glycerol solutions by the addition of membranes (5,10). This is not observed in the absence of osmolyte, indicating that a certain degree of helicity is necessary for the proteins to interact with membranes. In agreement with the subcellular localization of the proteins, liposomes containing a high fraction of chloroplast glycolipids were stabilized by COR15 proteins during a freeze-thaw cycle, in line with their physiological role as in vivo membrane stabilizers under such conditions (5,10).

Evidence for direct interactions between COR15 proteins and membranes has been obtained for mixed membranes in the dry state by Fourier-transform infrared (FTIR) spectroscopy (15), for pure phospholipid membranes in the presence of 50% glycerol by x-ray scattering (5), and during mild dehydration (equilibration at 97 or 75% relative humidity) by neutron membrane diffraction measurements (16). Because all previous evidence suggests that COR15A and COR15B are physiologically redundant and show the same folding behavior (5,11,15), we have concentrated our efforts in this study on COR15A. We have used coarse-grained MD simulations and FTIR spectroscopy to answer the following questions that had remained unresolved in previous work: 1) what is the relationship between COR15A folding and membrane binding? Is folding necessary for binding and is binding dependent on a particular orientation of the amphipathic helices with respect to the membrane surface? 2) Which amino acids interact with the membrane and what type of interaction (hydrophobic, ionic, polar) is responsible for membrane binding? 3) Is there lipid specificity in the binding of COR15A to membranes? 4) Does binding of COR15A to membranes influence the physical state of the membrane (lipid mixing, lipid dynamics)?

MATERIALS AND METHODS

Coarse-grained simulation of COR15A and membranes

Coarse-grained (CG) representations of the involved molecules were used. By coarse graining, the number of atoms of a system is reduced by creating pseudoatoms/beads, thus reducing the degrees of freedom of the overall system. This decreases the computational cost of the simulations, allowing longer simulation times. We used the Martini force fields (17) to model both the different lipid molecules (18) and the protein (19). To reduce the degrees of freedom of the system, the Martini force field creates a four-to-one mapping, in which on average four heavy atoms and associated hydrogens are represented by a single interaction center (bead), for which four main types of beads are defined: polar, nonpolar,

apolar, and charged. The interactions between particles are defined by Lennard-Jones potentials that can be used to estimate interaction energies between amino acids and lipid molecules (17). For the simulations of COR15A interaction with membranes, the polarizable Martini 2.2p protein force field (20,21) was used with a relative permittivity of the medium of 2.5. Long range electrostatic interactions beyond the real-space cutoff of 1.2 nm were treated using a shift method (22). All production runs were performed using the default Martini cutoffs with the parameter set "new-ref" (23). The script martinize.py v2.5 was used to create the CG representations of the molecules.

As templates for the COR15A structures, we used the atomistic models previously derived from MD simulations described recently that yielded a helix-loop-helix structure for the fully folded protein (11). To evaluate how the folding state of COR15A influences its membrane adsorption, three different conformations of the protein were used: folded, partially folded, and unfolded. For folded, we used the structure obtained by a comparative modeling approach in vacuo, yielding 46% α-helix content. For partially folded, the structure after 30 ns of MD simulation in the presence of 40% glycerol was used, resulting in 35% α-helix content, whereas for unfolded, the structure after 30 ns of MD simulation in water was used, containing 20% α-helix. The structures were constrained during the simulations to avoid unfolding of the protein in water (11). Protein flexibility was determined by analysis of the root mean-square deviation of the backbone of the protein, using the module g_rms of GROMACS 5.0.x.

To investigate the lipid specificity of the COR15A-membrane interactions, five different lipid molecules were used: 1-palmitoyl-2-oleoyl-sn-glycero-3-phosphatidylcholine (POPC, 16:0, 18:1), unsaturated monogalactosyldiacylglycerol (MGDG(U), 18:3, 18:3), saturated MGDG (MGDG(S) 18:0, 18:0), digalactosyldiacylglycerol (DGDG, 18:3, 18:3), and sulfoquinovosyldiacylglycerol (SQDG, 18:3, 16:0). Details of the headgroup structure of the three glycolipids are shown in Fig. S1. To approximate the composition of the native chloroplast membrane that would be the target of COR15A, we used a slightly simplified inner chloroplast mimicking membrane (ICMM) lipid composition (10) of 40% MGDG(U), 30% DGDG, and 30% SQDG, using published lipid parameters (24,25).

To create each system (COR15A + membrane + water or membrane + water), the "insane" script (26) was used. A box of 100 × 100 × 150 Å with ~340 lipids was created using periodic boundary conditions. The temperature was kept at 300 K by weak coupling to an external heat bath using the Berendsen thermostat (27) with a relaxation time of 2 ps. The pressure was maintained by weak coupling to an external reference pressure of 1.0 bar using a Berendsen barostat (27) with a compressibility of 3×10^{-4} bar^{-1} and a time constant of 1 ps. The time step for integration of the equations of motion was 20 fs, and the center of mass (COM) motion was removed linearly every 10 steps. In the systems including COR15A, the protein was positioned 60 Å from its COM to the COM of the bilayer. Four different orientations of COR15A relative to the membrane surface were used by rotating the protein along its long axis parallel to the bilayer, where 0° corresponds to the hydrophilic faces of the α-helices oriented toward the bilayer surface, whereas the 180° configuration had the hydrophobic faces toward the membrane (Fig. 1 C). GROMACS 5.0.x (28,29) was used to set up, launch, and analyze the coarse-grained MD (CGMD) simulations.

Additional simulations of 10 μs duration were performed in a bigger system in a box of 250 × 250 × 120 Å with 2046 lipid molecules and between two and six folded COR15A molecules. To reduce the computational time needed for the simulation of these large systems, proteins were positioned with their COM at a distance of 40 Å with respect to the COM of the membranes to reduce the total number of water molecules.

Before creating the mixed membranes used for the protein interaction analysis, four different bilayers consisting of pure lipids POPC, MGDG(S), DGDG, and SQDG were constructed. For each system, three replicates of 2 μs of CGMD simulations were performed, from which the first μs was discarded as an equilibration step. Structural parameters, such as the area
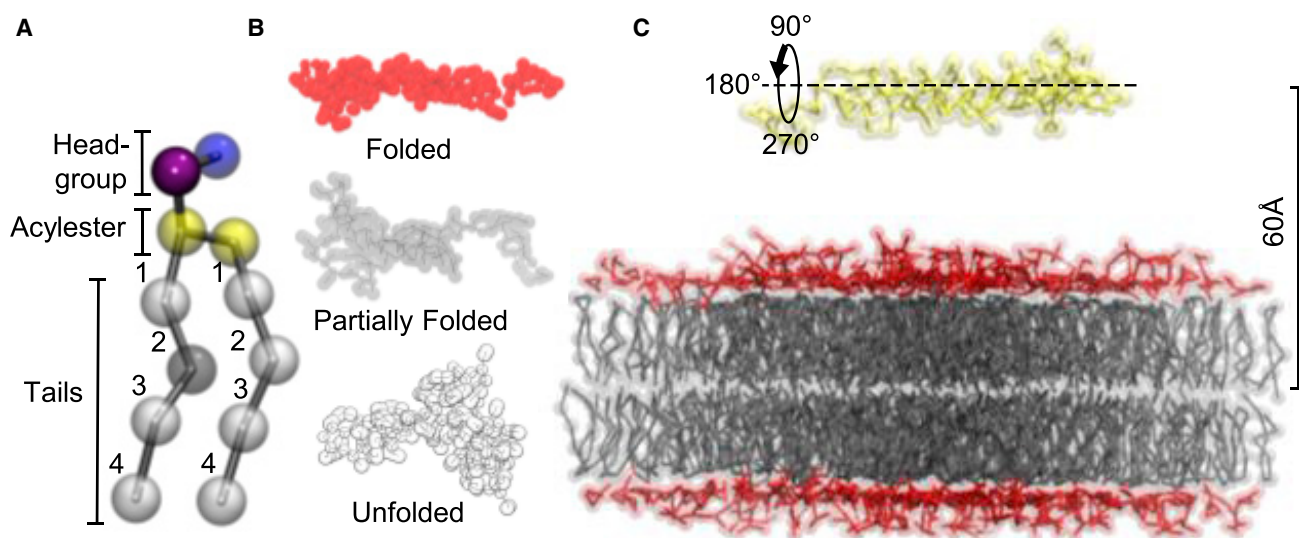
FIGURE 1 Schematic representation of the coarse-grained MD model. (*A*) Details of the lipid model are shown. Tails, glycerol backbone, and headgroup of the lipid POPC are represented in gray, yellow, blue, and cyan. The second bead in the fatty acyl tail is drawn in dark gray to indicate the presence of a double bond. Details of the glycolipids (headgroup structures and CG models) are shown in Fig. S1. (*B*) Models of COR15A in the folded, partially folded, and unfolded states are shown. (*C*) A representation of COR15A at configurations of 0, 90, 180, and 270° relative to the membrane surface is shown. 0° refers to an orientation of the hydrophilic faces of the protein α-helices toward the membrane surface. Of the 50 simulations of 200 ns each, 13 were at the 0° configuration, 13 at 90°, 12 at 180°, and 12 at 270°.

per lipid (average bilayer area divided by the number of lipids per leaflet) and membrane thickness (average distance between the headgroup beads in the opposing bilayer leaflets) were evaluated for each membrane using the GridMAT-MD tool (30) to validate the results in comparison with previous experimental and theoretical studies.

For adsorption simulations, 50 CGMD replicates were launched, each having a length of 200 ns. A protein was scored as "adsorbed" when it was attached to the membrane, irrespective of whether the whole protein was interacting with the membrane or only part of the protein. To estimate the adsorption differences in the protein-membrane systems, the Kaplan-Meier survival function (31) was used in the R package "survival," in which each "death" in the survival function corresponded to an adsorption event. Because no dissociation events were observed during the 200 ns run time of the simulations when protein binding had occurred, adsorption events could be summed up over the 50 simulation replicates. The significance of differences among adsorption curves was tested with the G-ρ test (32) using the R package "survival." To quantify the involvement of different amino acid residues in COR15A in the protein-membrane interaction, we determined the average number of lipid and water molecules within a radius of 10 Å around each amino acid side chain at the end of the 50 simulations. We then calculated the probability of a given amino acid side chain interacting with lipid or water molecules.

To analyze the fatty-acyl-tail order of the different lipids, we estimated the second-rank order parameter, which is defined as

$$P = \frac{1}{2}\left(3cos^2\langle\theta\rangle - 1\right), \tag{1}$$

where θ is the angle between the bonds and the bilayer normal (*z* axis). $P = 1$ would indicate a perfect alignment of the bonds with respect to the bilayer normal, whereas $P = 0$ would indicate a random orientation of the tail groups.

Lateral diffusion of the lipid molecules was calculated from their mean-square displacement in the membrane plane as

$$MSD = \left\langle |r(t + t_0) - r(t_0)|^2 \right\rangle, \tag{2}$$

where *r* represents the position of the COM of a given molecule and the angular brackets indicate an average over both the simulation time t and the number of analyzed molecules.

The compressibility modulus K_A was calculated as

$$K_A = kT\langle A\rangle\left(N\left\langle(A - A_0)^2\right\rangle\right)^{-1}, \tag{3}$$

where *N* corresponds to the total number of lipids per leaflet and A_0 to the equilibrium area (18). In the 200 ns simulations, only the last 150 ns were used for the determination of K_A. Likewise, in the 10 μs simulations, only the last 8 μs were used.

In total, 600 simulations of 200 ns each and six simulations of 10 μs each were performed on different COR15A-membrane systems. Additional simulations were performed on pure lipid systems (Fig. S3; Table 1), yielding a total of more than 192 μs of CGMD simulations.

FTIR spectroscopy

MGDG, DGDG, SQDG, and egg phosphatidylglycerol (EPG) were purchased from Lipid Products (Redhill, Surrey, UK). The ICMM liposomes used in the experiments contained 40% (w/w) MGDG, 30% (w/w) DGDG, 15% (w/w) SQDG, and 15% (w/w) EPG (33). Samples contained either only liposomes or liposomes and recombinant COR15A (10) at a 1:4 (protein/lipid) mass ratio. Samples were dried under vacuum and then rehydrated over saturated solutions of different salts, yielding the relative humidities (RHs) indicated in the figure. Sample preparation has been described in detail recently (16). FTIR spectra were recorded from 4000 to 900 cm^{-1} with a Nicolet iS10 (Thermo Scientific, Waltham, MA) FTIR spectrometer. Sixteen spectra were coadded and analyzed using the Spectrum 10.4.3 software (PerkinElmer, Rodgau, Germany). Infrared spectra were smoothed using a smoothing factor of 20. Because the OH absorbance peak of water overlaps with the amide I peak, the water band of samples containing only liposomes were subtracted from protein/lipid mixtures at the respective RHs as described (16). At least three samples per condition were analyzed.

TABLE 1   Structural Parameters of Bilayers Formed by POPC, Fully Saturated MGDG, DGDG, and SQDG Calculated from Our CGMD Simulations and Comparison with Theoretical and Experimental Data ± SD

Lipid	Area Per Lipid (nm^2)			Membrane Thickness (nm)		
	Calculated	Theoretical	Experimental	Calculated	Theoretical	Experimental
POPC	0.65 ± 0.01	0.64 ± 0.09[a]	0.63 ± 0.13[b]	3.9 ± 0.2	3.8 ± 0.5[a]	4.0 ± 0.1[b]
MGDG	0.58 ± 0.01	0.62 ± 0.01[c]	–	4.4 ± 0.3	4.0 ± 0.1[c]	–
DGDG	0.63 ± 0.01	0.64 ± 0.01[c]	–	4.4 ± 0.3	4.1 ± 0.1[c]	–
SQDG	0.58 ± 0.01	0.58 ± 0.07[c]	–	4.4 ± 0.2	4.5 ± 0.1[c]	–

[a]Data are from (43).
[b]Data are from (44).
[c]Data are from (24). The error indicated for membrane thickness is the upper limit indicated by the authors.

RESULTS

In plant cells, the COR15 proteins are localized in chloroplasts (34–36). Therefore, the membranes that these proteins can potentially interact with during freezing have an unusual lipid composition, as they mainly contain the highly unsaturated glycolipids MGDG, DGDG, and SQDG, with a high proportion of the nonbilayer lipid MGDG(U) (37,38). For CGMD modeling, we used the Martini force field, which employs a four-to-one mapping in which on average four heavy atoms and associated hydrogens are represented by a single bead, providing a simplified representation of the lipid molecules (Fig. 1 A; Fig. S1). To validate the CGMD models of the membranes to be used in the modeling of COR15A-membrane interactions, we first performed 2 μs simulations with the pure lipid membranes in water and determined the area per lipid and bilayer thickness. Because the highly unsaturated MGDG(U) does not form bilayers, we used the saturated form of this lipid (MGDG(S)) to obtain MGDG bilayers for these purposes (38,39). The data we obtained from these pure lipid systems were in good agreement with previous theoretical and experimental analyses (Table 1). This indicates that the parameters used to model these glycolipid-rich bilayers are suitable to further investigate the interaction of COR15A with these membranes.

Folding increases interaction of COR15A with a glycolipid bilayer

To model the interaction propensity of COR15A with membranes, we started with a membrane lipid composition similar to that of chloroplast membranes (40% MGDG(U), 30% DGDG, 30% SQDG) that we refer to as ICMM. Because experimental studies indicated that folding may be a prerequisite for COR15A-membrane interaction (5,10), we used the folded, partially folded, and unfolded structures of the protein (Fig. 1 B) derived from our previous atomistic MD simulations (11) for our CGMD binding studies. Because COR15A rapidly unfolds when transferred into water (11), we restrained the protein structure to be able to investigate the influence of the folding state on membrane binding. However, the restrained structures were still not

rigid and showed a degree of flexibility when expressed as the root mean-square deviation of the protein backbone beads (Fig. S2). In addition, the COR15A molecules were placed above the membranes in four different orientations by rotation around the long axis of the helix-loop-helix structure (Fig. 1 C). The 0° orientation was defined as the folded protein positioned with the hydrophilic faces of the amphipathic α-helices facing the membrane surface. Because we used periodic boundary conditions, the protein molecule may be displaced along the z axis when it moves beyond the walls of the box. This can result in the protein appearing "below" the membrane with an opposite orientation relative to the membrane surface compared to the starting configuration. Because we were particularly interested in the effect of protein orientation on membrane binding, we did not include binding events of the protein that were affected by the periodic boundary conditions in any further analyses.

On average, over the 50 simulations in four different orientations, 20% of unfolded, 38% of partially folded, and 43% of folded protein molecules had adsorbed onto the ICMM bilayer at the end of the 200 ns simulations. This indicates that COR15A has to be at least partially folded to efficiently interact with membranes, in agreement with our previous experimental data (5,10). In addition, the orientation of the protein relative to the membrane surface also played an important role in adsorption, indicating that the fully folded protein interacted most efficiently when the hydrophobic faces of the helices were oriented toward the membrane surface (Fig. 2). In the partially folded and the unfolded protein, this orientation was no longer dominating the interactions.

The fact that COR15A bound to the membrane from all four starting orientations but with different efficiencies could indicate either that the protein can bind to the membrane in different orientations, i.e., by interacting with the membrane through different amino acids, or that the protein needed to reorient before binding in all but the 180° cases. To distinguish between these possibilities, we determined the ratio of lipid and water molecules within 10 Å from each amino acid residue in COR15A (Fig. 3). The analysis indicates that for all starting orientations of the fully folded protein (Fig. 3 A), the interactions between membrane and
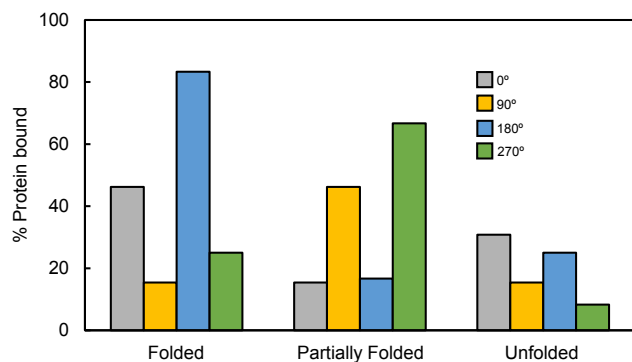
FIGURE 2 Fraction of simulations (in %) that produced a binding event of COR15A to the membrane from different starting configurations. The protein was either folded, partially folded, or unfolded during the simulation runs. For each of these conformations, 50 simulations of 200 ns were performed, of which 13 started with the hydrophilic faces of the amphipathic α-helices oriented toward the membrane surface (0° orientation), 13 with a 90°, 12 with a 180°, and 12 with a 270° rotation around the long axis of the protein (compare Fig. 1).

protein are mainly characterized by an insertion of the hydrophobic amino acids in the amphipathic α-helices between the lipids. This suggests that the protein is reorienting with its hydrophobic helix faces oriented toward the membrane to affect binding. Interestingly, there are two

hydrophobic amino acids in the central loop region of the fully folded protein that also show strong interactions with the lipids. These interactions are much less prominent in the partially or completely unfolded protein and may have an important role in membrane binding. In the partially folded state (Fig. 3 B), a similar picture emerges, although for the 0° starting orientation in particular, much less interaction is observed for the central part of the protein, which spans the loop region between the two helices (11). For the unfolded protein, the situation is not as clear as for the folded or partially folded protein (Fig. 3 C). This is probably due to the fact that fewer simulations could be included in the analysis because many fewer binding events were observed for the unfolded protein (Fig. 2). Nevertheless, it is clear from Fig. 3 that the unfolded protein also mainly interacted with the membrane through its hydrophobic amino acids.

Finally, we determined whether COR15A interacted preferentially with any of the glycolipids MGDG(U), DGDG, or SQDG (Fig. 4 A). SQDG showed the lowest interaction with the protein, whereas MGDG(U) and DGDG showed approximately equal degrees of interaction. Interestingly, this pattern was the same for the folded, partially folded, and unfolded protein, indicating that although folding determined the overall degree of binding of the protein to the
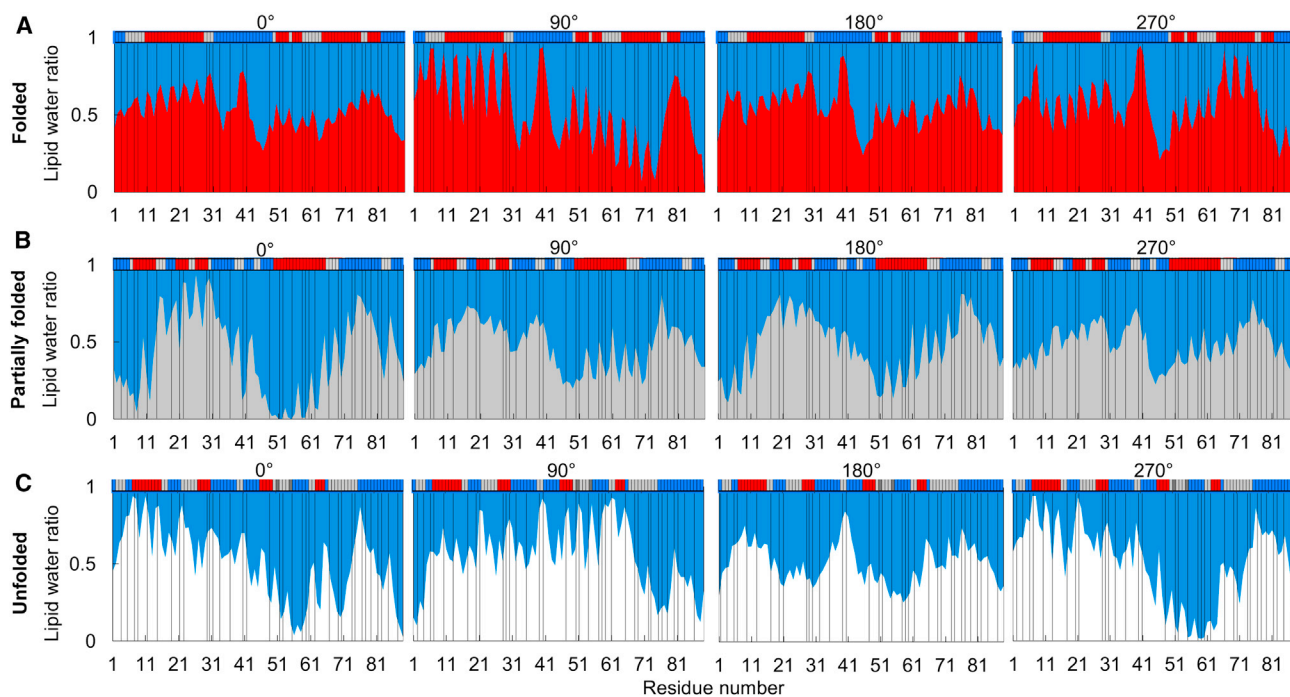

FIGURE 3 Preference of the amino acids in COR15A to interact either with water (blue) or lipid. This preference was determined from the average number of lipid and water molecules within a radius of 10 Å around each amino acid side chain at the end of the simulations. COR15A was either in a folded (red) (A), partially folded (gray) (B), or unfolded (white) (C) state in four different orientations relative to the membrane surface (compare Fig. 1). Only simulations in which the protein had bound to the membrane were considered for this analysis. Vertical black lines indicate the positions of hydrophobic amino acids in the protein. The squares on top of the panels indicate the localization of α-helical structure (red), turns (gray), and unfolded domains (blue). This structural information is taken from our previous atomistic MD simulations (11) of COR15A in vacuo (folded), in 40% glycerol (partially folded), and in water (unfolded).
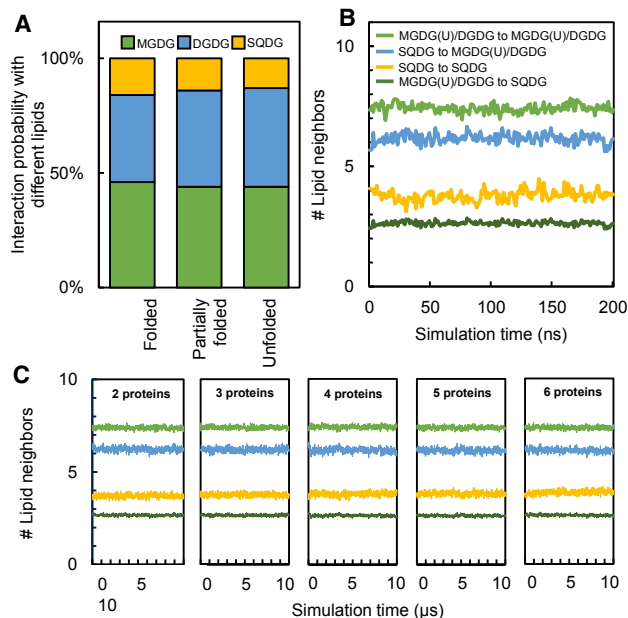
FIGURE 4 COR15A (*Folded*, *Partially Folded*, *Unfolded*) shows differential interaction with different lipids. (*A*) Differences in the probability of COR15A to interact with MGDG, DGDG, or SQDG in a mixed ICMM membrane (40% MGDG(U), 30% DGDG, 30% SQDG) are shown. (*B*) A nearest-neighbor analysis of ICMM lipids in the absence of COR15A during 200 ns simulation is shown. (*C*) A nearest-neighbor analysis of ICMM lipids in the presence of two to six protein molecules over a simulation time of 10 μs is shown. In (*B*) and (*C*), the color codes are identical.

membrane, the main interacting amino acids and lipids remained the same irrespective of the protein folding state. The preference of COR15A to interact with the galactolipids could have been due to a demixing of MGDG(U)/DGDG from SQDG before protein binding. However, a nearest-neighbor analysis showed clearly that during the 200 ns simulation time, in the absence of the protein, no such demixing occurred (Fig. 4 *B*). Alternatively, the adsorption of the protein and its preferential lipid interaction could have triggered a demixing of SQDG from the two galactolipid species. To answer this question comprehensively, we constructed a larger simulation system and monitored the nearest neighbor distribution of the lipids in the presence of 2, 3, 4, 5, or 6 protein molecules over a simulation time of 10 μs. Again, we did not find any indication for lipid demixing, indicating that preferential lipid interactions of the protein molecules had no influence on the average lipid distribution (Fig. 4 *C*).

Although COR15A adsorption did not lead to lipid demixing in ICMM membranes, it nevertheless had a marked influence on the physical behavior of the lipids. Fig. 5 shows that the lateral diffusion of all three lipid species was significantly reduced with an increasing number of bound protein molecules ($p = 0.0001$ for MGDG(U) and DGDG, $p = 0.0016$ for SQDG when comparing the membranes without proteins and in the presence of six COR15A molecules).
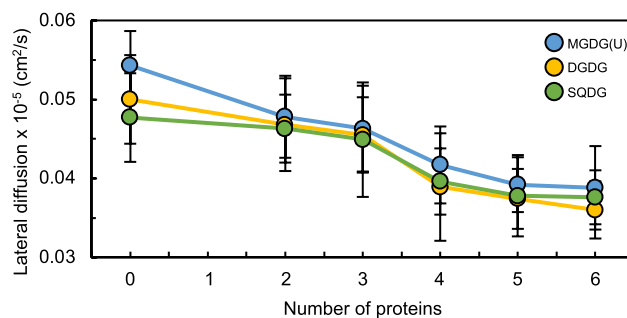

FIGURE 5 Adsorption of COR15A to ICMM membranes reduces lateral diffusion of the lipid molecules. The diffusion rates of MGDG(U), DGDG, and SQDG were determined in the presence of zero to six COR15A molecules. Error bars denote ± SD.

Although the nonbilayer lipid MGDG(U) showed the highest lateral diffusion rate in the absence of protein, with DGDG and SQDG showing progressively lower rates (differences between MGDG(U) and the other lipids significant at $p = 0.0269$), all three lipids already showed highly similar diffusion rates in the presence of two protein molecules. The lateral diffusion rates of all three lipids remained similar when further protein molecules were added, although the overall diffusion rate decreased further. This is in agreement with COR15A interacting with all three lipid types. Interactions of COR15A with the lipid fatty acids occurred mainly (40–45%) at the first bead of the chains, whereas interactions became progressively less frequent toward the center of the bilayer (Fig. S3).

We further used the simulations to calculate the compressibility modulus (K_A) of the ICMM membranes as a function of COR15A adsorption. The compressibility modulus defines the resistance of a membrane to a compressive force. When we compared the bilayer in the absence of protein with a bilayer with six bound COR15A molecules, we observed a significant (analysis of variance; ANOVA $p < 0.05$) reduction in K_A, from 68.07 ± 8.78 to 47.21 ± 3.40 mN m^{-1} (mean ± standard error (SE)). K_A was further determined from the simulations that were run with either the folded, partially folded, or unfolded protein in the presence of ICMM. Here, we either made the calculations from all 50 simulations with each protein conformation or only with those that resulted in a binding event (Table 2). K_A values were consistently lower when only simulations with binding events were considered, again indicating that protein binding reduced K_A. Interestingly, this was true for all three conformations of COR15A, indicating that the bound protein had a similar effect on membrane rigidity independent of its conformation. It should also be noted that the smaller bilayer patches used in these simulations (340 lipids) had a higher compressibility than the larger patches used for the absorption of up to six protein molecules (2046 lipids), in agreement with simulation data on dimyristoylphosphatidylcholine (DMPC) bilayers (18).

TABLE 2 Compressibility Modulus K_A of ICMM Bilayers Formed by 40% MGDG, 30% DGDG, and 30% SQDG Calculated from the 200 ns CGMD Simulations

	Folded	Partially Folded	Unfolded
All simulations	227.73 ± 9.94	310.23 ± 7.10	360.38 ± 9.22
Simulations with bound protein only	200.81 ± 22.23	274.67 ± 11.57	281.44 ± 15.57

K_A was either calculated from all 50 simulations (i.e., both those in which binding had occurred and those in which no binding of COR15A to the bilayers was observed) or only from those simulations that resulted in COR15A binding. The values (mN m^{-1}) denote means ± SE. ANOVA (analysis of variance) indicated that the values for the folded, partially folded, and unfolded protein were significantly different at $p < 0.001$ for all simulations and at $p < 0.01$ when only simulations with bound protein were considered.

MGDG(U) and DGDG show phase separation from POPC during simulation

To study the role of the different thylakoid glycolipids in the adsorption of COR15A separately for each lipid species, several membrane models were constructed that contained mixtures of the phospholipid POPC with the different glycolipids. Because the nonbilayer properties of MGDG depend strongly on the degree of unsaturation of its fatty acyl chains (39), in addition to the naturally occurring highly unsaturated MGDG (MGDG(U)), we also included a fully saturated version (MGDG(S)) in our analyses. In all cases, the membranes contained equal numbers of POPC and glycolipid molecules.

Before adding the protein into the system, we ran three replicates of 1 μs simulations of each mixed bilayer. Interestingly, unlike in the mixed ICMM system, here a clear phase separation was observed in the mixtures containing POPC and either DGDG or MGDG(U) (Fig. S4). During the first 50 ns, POPC was completely phase separated from DGDG or MGDG(U) into different domains, staying demixed through the remaining simulation time. On the other hand, in the simulations with POPC/MGDG(S), only partial demixing occurred, indicating the importance of fatty-acyl-chain unsaturation for this process. In the case of the negatively charged lipid SQDG, no phase separation from POPC was observed.

Binding of COR15A depends on membrane lipid composition

Next, we quantified the binding of COR15A to membranes with different lipid compositions (Fig. 6; Table S1). Because the fully folded protein showed the highest affinity for the ICMM, only this state of the protein was used for the following adsorption analyses. In addition, because we observed no differences in adsorption between the different orientations of the protein relative to the bilayer (analysis not shown), the mean of all 50 simulations combining all four orientations is presented.
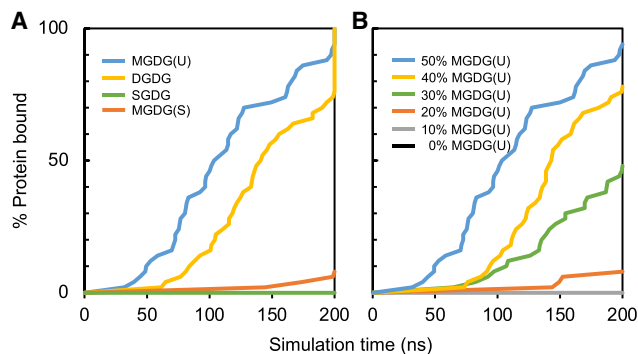

FIGURE 6 Adsorption of folded COR15A to membranes. Membranes in (A) were made from equimolar mixtures of POPC with MGDG(U), DGDG, SQDG, or MGDG(S). Membranes in (B) were made from 100% POPC, 90% POPC/10% MGDG(U), 80% POPC/20% MGDG(U), 70% POPC/30% MGDG(U), 60% POPC/40% MGDG(U), and 50% POPC/50% MGDG(U). See Table S1 for further details. Because no binding was observed with 100% POPC and 90% POPC/10% MGDG(U), only the latter curve is visible in (B).

The adsorption of COR15A onto ICMM indicated a higher affinity of the protein for MGDG(U) and DGDG than to SQDG (Fig. 4). In agreement with these data, COR15A was unable to adsorb onto membranes composed of POPC/SQDG (Fig. 6 A). On the other hand, with membranes composed of POPC and either MGDG(U) or DGDG, the adsorption events increased significantly, reaching 92 and 74%, respectively. The fact that with bilayers formed by POPC/MGDG(S) only three out of 50 simulations resulted in protein adsorption (Table S1) indicates that fatty-acyl-chain unsaturation is a decisive factor for binding. Adsorption of COR15A to membranes was a direct function of the fraction of MGDG(U) in POPC membranes (Fig. 6 B). Although 20% MGDG(U) was not sufficient for effective protein adsorption (only 3 out of 50 simulations resulted in binding after 200 ns; Table S1), this was strongly increased for 30% MGDG(U) (24 out of 50 simulations) and reached 48 binding events in 50 simulations in the presence of 50% MGDG(U)/50% POPC.

Similar to the binding to ICMM membranes, binding to membranes containing 50% MGDG(U)/50% POPC also involved interactions between the membrane lipids and hydrophobic amino acids (Fig. S5). However, hydrophobic interactions between COR15A and lipids were not the only contribution to membrane adsorption. To fully assess the contributions of charged, polar, and hydrophobic interactions to the energetics of the protein-membrane interaction, we extended a single simulation from the 50 replicas in which an adsorption event had occurred for lipid compositions of 50% MGDG(U) or MGDG(S) and 50% POPC from 200 ns to 1 μs. The analysis showed that although interactions of hydrophobic amino acids with MGDG(U) accounted for a significant fraction of the total binding energy, charged and polar amino acids together provided two-thirds of the total energy (Fig. 7). In the case of
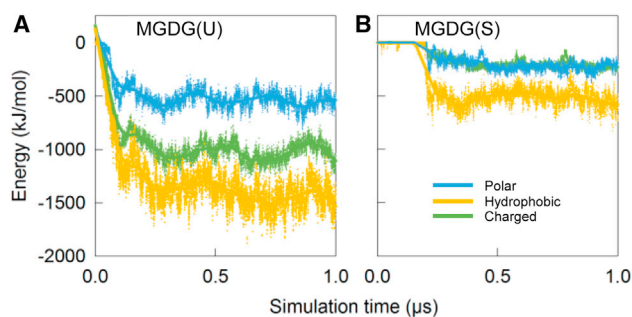
FIGURE 7 Interaction of charged, hydrophobic, and polar amino acids of fully folded COR15A with MGDG(U) (*A*) and MGDG(S) (*B*) in mixed MGDG/POPC membranes containing either unsaturated MGDG(U) or fully saturated MGDG(S). The contribution of the different classes of amino acids to the binding energy of the protein to the membrane is plotted as a function of the simulation time up to 1 μs.

MGDG(S), the contribution of hydrophobic amino acids was very low, and only charged amino acids contributed significantly to the binding energy. This may indicate that in the presence of saturated lipids, insertion of the protein into the membrane was more shallow, allowing mainly interactions between the lipid headgroup and the protein.

We therefore wanted to know whether the interactions of COR15A with the different lipids had an influence on the fatty-acyl-chain dynamics. Hence, we quantified these dynamics as the average order parameters of both fatty acyl chains of each lipid in the absence and presence of an adsorbed COR15A molecule. We again extended a single simulation from the 50 replicas in which an adsorption event had occurred from 200 ns to 1 μs. In those systems in which no protein adsorption could be observed (POPC and POPC/SQDG; compare Fig. 5), order parameters could only be determined without protein. In all cases, the order parameter decreased from the membrane surface (bead 1) toward the membrane center (bead 4) (Fig. 8). In addition, the relatively saturated lipids MGDG(S) and POPC showed the highest
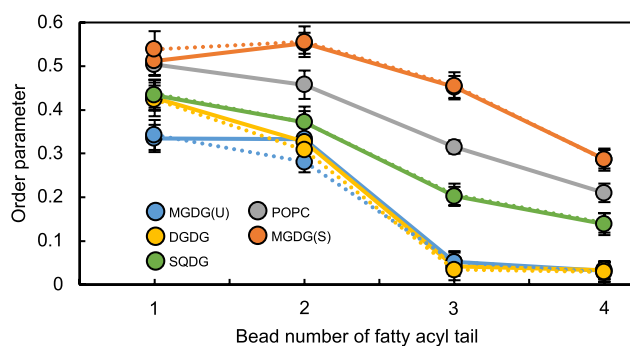

FIGURE 8 Order parameter analysis of lipids in pure POPC or POPC/glycolipid membranes. Average order parameters obtained from the beads of the two fatty acyl tails of the lipids (compare Fig. 1 *A*) are depicted for MGDG(U), DGDG, SQDG, POPC, and MGDG(S). Solid lines indicate measurements in systems without protein, and dotted lines indicate the presence of membrane-bound COR15A. Error bars denote ± SD.

order parameters, whereas highly unsaturated MGDG(U) and DGDG showed the lowest order parameters. For these two lipids, the binding of COR15A decreased the order parameter specifically at the second bead, indicating increased spacing and a higher free volume in this part of the bilayer. In contrast, MGDG(S) showed a higher order parameter specifically at the first bead, indicating a more shallow interaction, in agreement with the interaction energies as described above (Fig. 7).

Folding of COR15A is increased more by ICMM than pure POPC liposomes

The simulation data clearly indicate that COR15A binds much more efficiently to ICMM than to pure POPC bilayers. To test this prediction experimentally, we measured the secondary structure of recombinant COR15A by FTIR spectroscopy in the presence of ICMM liposomes. For this analysis, the samples were first dried under vacuum and then equilibrated at different RHs over saturated solutions of different salts (40). We subsequently evaluated the amide I peaks of the FTIR spectra of the different samples that contain information about the secondary structure of the protein (41,42). At 100% RH (i.e., equilibration over D_2O), COR15A showed an amide I peak at $\sim$1644 cm^{-1}, indicating a largely unstructured state of the protein (Fig. 9). With a progressive reduction in RH, the amide I peak shifted to higher wavenumbers, up to $\sim$1655 cm^{-1}, in agreement with the previously shown folding of COR15A into α-helices (11,15). Comparison of the amide I peak positions of COR15A in the presence of ICMM at different RHs with previously published data (16) for the pure protein and COR15A in the presence of POPC liposomes (Fig. 9) indicates the presence of more α-helix content in the protein in the presence of ICMM membranes, in agreement with the predictions from the simulations reported above.

DISCUSSION

Properties of the simulated bilayers

We have used CGMD simulations to investigate interactions between the COR15A protein and membranes of different lipid composition. Within these simulations, we determined various membrane parameters (area per lipid, bilayer thickness, lateral lipid diffusion, lipid order parameters, lipid mixing, and phase separation) in the absence of the protein, and we will first discuss these before discussing the factors affecting COR15A-membrane binding and its effect on membrane properties.

The data on area per lipid and bilayer thickness we obtained from the pure lipid systems are in good agreement with previous theoretical (24) and experimental (43,44) analyses. The lateral lipid diffusion rates we determined for
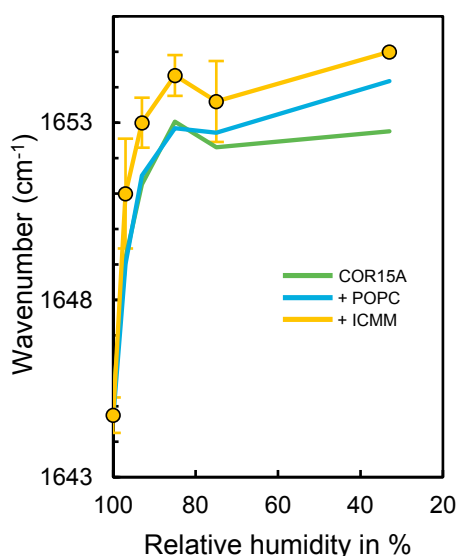
FIGURE 9 Impact of POPC and ICMM liposomes on the folding of COR15A at different relative humidities (% RHs). Protein secondary structure was investigated using FTIR spectroscopy. The position of the amide I peak maximum of COR15A is shown as an indication of secondary structure content. A 1:4 protein/lipid mass ratio was used for all measurement. The amide I peak position $\pm$ SD of at least three replicate measurements is shown for samples containing ICMM liposomes. Curves indicating corresponding measurements with pure COR15A or COR15A in the presence of POPC liposomes were taken from a recent publication (16).

the ICMM membranes are consistent with the rates determined by CGMD simulations of phospholipids (45) and of lipids in a more complex thylakoid lipid mixture (25). The latter study found, in agreement with our analysis, that polyunsaturated lipids show slightly faster diffusion rates than saturated lipids and that lipids with an identical degree of unsaturation but with a larger headgroup (DGDG) diffuse more slowly than those with a smaller headgroup (MGDG(U)). Lipid diffusion measurements in thylakoid membranes of a cyanobacterium, on the other hand, yielded diffusion constants that were ~100-fold lower. However, the lipids in these membranes are largely saturated, and in addition, these membranes contain a very high proportion of intrinsic membrane proteins that will slow down lipid diffusion compared to a pure lipid membrane (46).

The compressibility modulus for ICMM membranes that we determined in the presence of the unfolded protein (50 simulations $\sim$ 20% binding events; $K_A = 360$ mN m^{-1}) was similar to the value of 400 mN m^{-1} reported for a similarly sized bilayer patch (260 lipids) of DMPC (18). Interestingly, although K_A decreased to 260 mN m^{-1} when the bilayer patch of DMPC was larger (6400 lipids), this decrease was much more drastic for the larger ICMM bilayer, for which a simulation with 2046 lipids resulted in a K_A value of only 68 mN m^{-1}. Why the glycolipid-rich, highly unsaturated bilayers responded much more strongly to the increase in model membrane size remains to be elucidated.

The fatty-acyl-chain order parameters decreased from the membrane surface toward the membrane center. The same dependence has been found in a previous CGMD study (25) as well as in an atomistic MD simulation (47) and experimentally by electron spin resonance (48) and NMR (47,49) spectroscopy. A theoretical analysis of this phenomenon has been presented previously (50). The order parameters that we determined are quantitatively and qualitatively similar to those reported from another CGMD simulation (25).

In the ICMM membrane, we found a homogeneous distribution of all three lipid species, in agreement with a CGMD study of a similar thylakoid lipid membrane (25). However, membranes composed of 50% POPC and 50% of either MGDG(U) or DGDG showed complete lipid segregation into phospholipid and galactolipid domains. This could be driven by both the different headgroup structure (sugar versus phosphorylcholine) and/or the higher degree of unsaturation of the galactolipids. Because MGDG(U) showed a stronger separation from POPC than MGDG(S), the latter factor is clearly important. A contribution of sugar headgroups has, however, been suggested from a CGMD study of gangliosides in phospholipid membranes (51). In contrast to these CGMD results, it was found experimentally that equal mixtures of DMPC (a fully saturated PC, 14:0) and DGDG were completely mixed in the fully hydrated state (52) and only showed very moderate demixing in the dry state (53). Similarly, only weak demixing was found between DMPC and MGDG (the highly unsaturated form from green leaves) in dried liposomes (54), whereas no demixing was observed in an atomistic MD simulation of a fully hydrated bilayer of the same two lipids (55) or from NMR spectroscopy experiments (56). These data indicate that the force field used in our study tends to overestimate demixing between galactolipids and phospholipids. However, for our analysis of protein-membrane interactions, this should not be problematic because COR15A showed a strong preference to interact with the polyunsaturated galactolipids both in the well-mixed ICMM membrane and the phase-separated POPC/MGDG(U) and POPC/DGDG membranes.

Factors determining COR15A-membrane interaction

Our simulation results clearly show that both the folding state of COR15A and membrane lipid composition determined the extent of membrane binding of the protein. Binding increased with increasing protein α-helix content, in agreement with a recent CGMD study on two 21-amino-acid model peptides (57). In our simulation system, protein structure was restrained to prohibit protein unfolding that would otherwise take place when the folded protein is suspended in water (11,15). However, the restrained structures still displayed a similar degree of flexibility, as we observed

in a previous atomistic simulation in which the folded, partially folded, and unfolded protein were modeled in vacuo, in 40% glycerol, and in water, respectively (11). This situation obviously cannot be exactly replicated in experiments. However, there is indirect evidence that at least partial folding is also necessary for membrane binding under different experimental conditions. Experimentally, different degrees of folding can be induced in COR15A by either glycerol-induced crowding (11) or by gradual rehydration of the fully folded, dry protein at different RHs (16). Indirect evidence for membrane binding is obtained by adding liposomes to the crowded system, which leads to an increase in protein folding (10). Following the same logic, we have shown here that the presence of ICMM liposomes increased COR15A folding under partially dehydrated but not under fully hydrated conditions. Induced folding of an IDP due to membrane binding has previously been shown also for example, for α-synuclein, a mammalian protein of similar size involved in the neuropathology of Parkinson's disease (58–60), and for the *Arabidopsis* protein LEA18 (61), indicating a wider relevance for such a mechanism. It should, however, be pointed out that in these latter cases, the initial binding of the unfolded protein to the membrane is driven by electrostatic interactions between the positively charged protein and acidic lipids such as phosphatidylserine or phosphatidylglycerol. COR15A, on the other hand, is negatively charged and consequently showed a depletion of SQDG among its nearest neighbor lipids when bound to ICMM membranes. In addition, it did not bind to POPC/SQDG membranes but rather required highly unsaturated galactolipids. Consequently, approximately two-thirds of the binding energy between protein and membrane was contributed by polar and charged amino acids. The remaining third of the interaction energy was contributed by hydrophobic amino acids. This is in agreement with the fact that COR15A folds into an amphipathic α-helix (11,15) and that the hydrophobic amino acids were in closest contact with the lipid molecules in the membrane-bound state. Interestingly, this was even true for the progressively more unfolded COR15A proteins, indicating that these hydrophobic interactions are essential for membrane binding. Also, the fact that increased folding of the protein into amphipathic α-helices resulted in enhanced membrane binding indicates the importance of a hydrophobic interface on the protein for its interaction with membranes.

An additional requirement for COR15A binding to membranes was the presence of polyunsaturated lipids. This is demonstrated by the fact that the protein only bound to membranes containing highly unsaturated DGDG or MGDG(U) but not to those containing saturated MGDG(S) or monounsaturated POPC. It has been shown that polyunsaturated phospholipids facilitate binding of the proteins dynamin and endophilin to membranes, thereby increasing membrane deformation and vesicle fission (62). These findings are in agreement with the idea that accessibility of a membrane surface for proteins and peptides is largely governed by the frequency and depth of lipid packing defects (63–65) due to the presence of polyunsaturated bilayer and nonbilayer lipids that induce spontaneous membrane curvature (64–66).

Neutron diffraction experiments showed that COR15A can also bind to POPC membranes (16), although this was not observed in our simulations. In addition, COR15A reduces the lipid phase transition temperature of anhydrous POPC, also indicating protein-lipid interaction (10,15). However, it should be noted that in the experimental system, the samples were dehydrated to induce protein folding, whereas in the simulations, a comparatively large water volume was present. The removal of water will obviously bring the protein into greater proximity to the membrane and could therefore induce interactions that would not occur in a situation in which the protein has sufficient aqueous space for diffusion.

Effects of COR15A binding on bilayer properties

Because experimental evidence shows a protective effect of COR15A for chloroplast membranes during freezing in vivo (5,67) and for ICMM liposomes in vitro (5,10), another interesting aspect of the current study concerns the influence of COR15A binding on membrane properties.

Our analysis showed that COR15A preferentially interacted with MGDG(U) and DGDG in ICMM, whereas it showed less interaction with SQDG. This can be easily rationalized by the fact that both SQDG and COR15A carry a net negative charge leading to mutual repulsion. However, this preferential interaction with MGDG(U) and DGDG did not lead to lipid demixing at the site of protein binding. Similarly, the positively charged proteins annexin a5 (68) and α-synuclein (69) do not induce lipid demixing upon peripheral binding to model membranes containing negatively charged lipids. Rather, both studies indicate transient interactions of lipids with the proteins and a rapid exchange between lipids directly in contact with the proteins and lipids in the bulk phase. Despite this, COR15A binding to ICMM resulted in a significant reduction in the rate of lateral diffusion of all three lipid species. This is in agreement with experimental studies of the effect of binding of annexin a5 and α-synuclein on lateral lipid diffusion (68,69). In addition to the reduction in lateral diffusion, we also found a significant reduction in the compressibility modulus of the ICMM membranes upon binding of COR15A, indicating a less-rigid bilayer.

Recent neutron membrane diffraction measurements indicate that in a dehydrated system, COR15A inserts between the lipid headgroups of POPC down to the first five to six carbon atoms of the fatty acyl chains (16). In agreement with this position, we found only small effects of COR15A binding on lipid order parameters. In particular, there were no effects on the order parameters of beads 3 and

4 at the center of the bilayer, indicating that the protein was indeed only peripherally interacting with the membranes, similar to the experimentally observed effects of peripherally bound α-synuclein (70,71). Also in agreement with these studies, we observed decreased order parameters of bead 2 specifically upon binding of COR15A to membranes containing MGDG(U) or DGDG. We interpret this as an increase in lipid spacing around the position of bead 2 due to the insertion of the protein at and directly below the glycerol backbone region of the membrane lipids, which is also indicated by the highest affinity of COR15A for bead 1 in all lipids of the ICMM membrane. This increase in lipid spacing is also consistent with the reduced membrane rigidity indicated by the reduced compressibility modulus of the membranes after protein binding. Interestingly, COR15A binding to membranes containing MGDG(S) resulted in a slightly increased order parameter at bead 1. This may be due to motional restriction of this bead caused by a shallower insertion of the protein between the saturated lipids, in agreement with the much smaller contribution of hydrophobic amino acids to the interaction energy in this case.

As indicated above, the physiological role of COR15A and its close homolog COR15B is the stabilization of chloroplast membranes during freezing. The analyses presented in this study, together with previous experimental and computational results, allow us to propose the most detailed mechanism of action for any LEA protein thus far. COR15A is induced under cold but nonfreezing conditions at the transcriptional level (72) and is imported into the chloroplast stroma, where it resides as an intrinsically disordered, soluble protein (34–36). Upon freezing, ice crystallization takes place in the apoplastic space and cells are dehydrated (73). Freeze-induced dehydration results in (partial) folding of COR15A (5,10,11,16), leading to membrane binding and additional folding (5,10). The high content of polyunsaturated MGDG in chloroplast membranes (37) leads to negative curvature stress, as unsaturated MGDG is a nonbilayer lipid that in isolation arranges in a hexagonal II phase in an aqueous environment (37–39). When MGDG is incorporated into a lipid bilayer, this makes the resulting membranes highly unstable under conditions such as freezing (33). The peripheral insertion of COR15A into these membranes alleviates the negative curvature stress and thus stabilizes the membranes. Collectively, these data indicate that the COR15 proteins are a protective system that has evolved to specifically stabilize chloroplast membranes with their unique lipid composition.

CONCLUSIONS

COR15A is a cold-induced IDP that contributes to the freezing tolerance of *A. thaliana* by stabilizing mainly the inner chloroplast envelope membrane. Our CGMD simulations indicate that at least partial folding of the protein is required for efficient interaction with membranes composed of chloroplast glycolipids because the hydrophobic amino acids located on the hydrophobic face of the amphipathic helices are important for membrane binding. On the other hand, the presence of highly unsaturated galactolipids in the membranes is necessary for adsorption even of the fully folded protein. This suggests that lipid packing defects in the membrane are necessary to allow the protein access between the lipid headgroups to hydrophobically interact with the upper parts of the fatty acyl chains. At the same time, this interaction reduces the negative curvature stress induced by the presence of a nonbilayer lipid such as MGDG(U) and stabilizes the membrane. Our work provides the first physical description, to our knowledge, of how an intrinsically disordered LEA protein interacts with and stabilizes a membrane. This provides a basis for further rational experimental and theoretical approaches that will allow us to understand the vast natural variability in these proteins and to optimize them for technical applications such as cell and tissue preservation.

SUPPORTING MATERIAL

AUTHOR CONTRIBUTIONS

C.N.-R., W.G., and D.K.H. conceived the project, and all authors participated in the design of computational strategies. A.B. performed the FTIR measurements and data analysis and prepared all figures. C.N.-R. and D.K.H. wrote the manuscript. All authors read the manuscript, edited, and commented on it before submission.

ACKNOWLEDGMENTS

REFERENCES

1. Guy, C., F. Kaplan, …, D. K. Hincha. 2008. Metabolomics of temperature stress. *Physiol. Plant.* 132:220–235.

2. Hincha, D. K., C. Espinoza, and E. Zuther. 2012. Transcriptomic and metabolomic approaches to the analysis of plant freezing tolerance and cold acclimation. *In* Improving Crop Resistance to Abiotic Stress. N. Tuteja, S. S. Gill, A. F. Tiburcio, and R. Tuteja, eds. Wiley-Blackwell, pp. 255–287.

3. Xin, Z., and J. Browse. 2000. Cold comfort farm: the acclimation of plants to freezing temperatures. *Plant Cell Environ.* 23:893–902.

4. Thomashow, M. F. 2010. Molecular basis of plant cold acclimation: insights gained from studying the CBF cold response pathway. *Plant Physiol.* 154:571–577.

5. Thalhammer, A., G. Bryant, …, D. K. Hincha. 2014. Disordered cold regulated15 proteins protect chloroplast membranes during freezing through binding and folding, but do not stabilize chloroplast enzymes in vivo. *Plant Physiol.* 166:190–201.

6. Hundertmark, M., and D. K. Hincha. 2008. LEA (late embryogenesis abundant) proteins and their encoding genes in *Arabidopsis thaliana*. *BMC Genomics.* 9:118.

7. Hand, S. C., M. A. Menze, …, D. Moore. 2011. LEA proteins during water stress: not just for plants anymore. *Annu. Rev. Physiol.* 73:115–134.

8. Tunnacliffe, A., D. K. Hincha, …, D. Macherel. 2010. LEA proteins: versatility of form and function. *In* Sleeping Beauties - Dormancy and Resistance in Harsh Environments. E. Lubzens, J. Cerda, and M. Clark, eds. Springer, pp. 91–108.

9. Hincha, D. K., and A. Thalhammer. 2012. LEA proteins: IDPs with versatile functions in cellular dehydration tolerance. *Biochem. Soc. Trans.* 40:1000–1003.

10. Bremer, A., M. Wolff, …, D. K. Hincha. 2017. Folding of intrinsically disordered plant LEA proteins is driven by glycerol-induced crowding and the presence of membranes. *FEBS J.* 284:919–936.

11. Navarro-Retamal, C., A. Bremer, …, A. Thalhammer. 2016. Molecular dynamics simulations and CD spectroscopy reveal hydration-induced unfolding of the intrinsically disordered LEA proteins COR15A and COR15B from *Arabidopsis thaliana*. *Phys. Chem. Chem. Phys.* 18:25806–25816.

12. Baskakov, I., and D. W. Bolen. 1998. Forcing thermodynamically unfolded proteins to fold. *J. Biol. Chem.* 273:4831–4834.

13. Chang, Y. C., and T. G. Oas. 2010. Osmolyte-induced folding of an intrinsically disordered protein: folding mechanism in the absence of ligand. *Biochemistry.* 49:5086–5096.

14. Qu, Y., C. L. Bolen, and D. W. Bolen. 1998. Osmolyte-driven contraction of a random coil protein. *Proc. Natl. Acad. Sci. USA.* 95:9268–9273.

15. Thalhammer, A., M. Hundertmark, …, D. K. Hincha. 2010. Interaction of two intrinsically disordered plant stress proteins (COR15A and COR15B) with lipid membranes in the dry state. *Biochim. Biophys. Acta.* 1798:1812–1820.

16. Bremer, A., B. Kent, …, D. K. Hincha. 2017. Intrinsically disordered stress protein COR15A resides at the membrane surface during dehydration. *Biophys. J.* 113:572–579.

17. Marrink, S. J., H. J. Risselada, …, A. H. de Vries. 2007. The MARTINI force field: coarse grained model for biomolecular simulations. *J. Phys. Chem. B.* 111:7812–7824.

18. Marrink, S. J., A. H. de Vries, and A. E. Mark. 2004. Coarse grained model for semiquantitative lipid simulations. *J. Phys. Chem. B.* 108:750–760.

19. Monticelli, L., S. K. Kandasamy, …, S. J. Marrink. 2008. The MARTINI coarse-grained force field: extension to proteins. *J. Chem. Theory Comput.* 4:819–834.

20. de Jong, D. H., G. Singh, …, S. J. Marrink. 2013. Improved parameters for the Martini coarse-grained protein force field. *J. Chem. Theory Comput.* 9:687–697.

21. Yesylevskyy, S. O., L. V. Schäfer, …, S. J. Marrink. 2010. Polarizable water model for the coarse-grained MARTINI force field. *PLoS Comput. Biol.* 6:e1000810.

22. van der Spoel, D., and P. J. van Maaren. 2006. The origin of layer structure artifacts in simulations of liquid water. *J. Chem. Theory Comput.* 2:1–11.

23. de Jong, D. H., S. Baoukina, …, S. J. Marrink. 2016. Martini straight: boosting performance using a shorter cutoff and GPUs. *Comput. Phys. Commun.* 199:1–7.

24. López, C. A., Z. Sovova, …, S. J. Marrink. 2013. Martini force field parameters for glycolipids. *J. Chem. Theory Comput.* 9:1694–1708.

25. van Eerden, F. J., D. H. de Jong, …, S. J. Marrink. 2015. Characterization of thylakoid lipid membranes from cyanobacteria and higher plants by molecular dynamics simulations. *Biochim. Biophys. Acta.* 1848:1319–1330.

26. Wassenaar, T. A., H. I. Ingólfsson, …, S. J. Marrink. 2015. Computational lipidomics with insane: a versatile tool for generating custom membranes for molecular simulations. *J. Chem. Theory Comput.* 11:2144–2155.

27. Berendsen, H. J. C., J. P. M. Postma, …, J. R. Haak. 1984. Molecular dynamics with coupling to an external bath. *J. Chem. Phys.* 81:3684–3690.

28. Abraham, M. J., T. Murtola, …, E. Lindahl. 2015. GROMACS: high performance molecular simulations through multi-level parallelism from laptops to supercomputers. *SoftwareX.* 1–2:19–25.

29. Pronk, S., S. Páll, …, E. Lindahl. 2013. GROMACS 4.5: a high-throughput and highly parallel open source molecular simulation toolkit. *Bioinformatics.* 29:845–854.

30. Allen, W. J., J. A. Lemkul, and D. R. Bevan. 2009. GridMAT-MD: a grid-based membrane analysis tool for use with molecular dynamics. *J. Comput. Chem.* 30:1952–1958.

31. Kaplan, E. L., and P. Meier. 1958. Nonparametric estimation from incomplete observations. *J. Amer. Statist. Assn.* 53:457–481.

32. Harrington, D. P., and T. R. Fleming. 1982. A class of rank test procedures for censored survival data. *Biometrika.* 69:553–566.

33. Hincha, D. K., A. E. Oliver, and J. H. Crowe. 1998. The effects of chloroplast lipids on the stability of liposomes during freezing and drying. *Biochim. Biophys. Acta.* 1368:150–160.

34. Candat, A., P. Poupart, …, D. Macherel. 2013. Experimental determination of organelle targeting-peptide cleavage sites using transient expression of green fluorescent protein translational fusions. *Anal. Biochem.* 434:44–51.

35. Lin, C., and M. F. Thomashow. 1992. DNA sequence analysis of a complementary DNA for cold-regulated *Arabidopsis* gene *cor15* and characterization of the COR15 polypeptide. *Plant Physiol.* 99:519–525.

36. Nakayama, K., K. Okawa, …, T. Inaba. 2007. Arabidopsis Cor15am is a chloroplast stromal protein that has cryoprotective activity and forms oligomers. *Plant Physiol.* 144:513–523.

37. Dörmann, P., and C. Benning. 2002. Galactolipids rule in seed plants. *Trends Plant Sci.* 7:112–118.

38. Webb, M. S., and B. R. Green. 1991. Biochemical and biophysical properties of thylakoid acyl lipids. *Biochim. Biophys. Acta.* 1060:133–158.

39. Gounaris, K., D. A. Mannock, …, P. J. Quinn. 1983. Polyunsaturated fatty acyl residues of galactolipids are involved in the control of bilayer/non-bilayer lipid transitions in higher plant chloroplasts. *Biochim. Biophys. Acta.* 732:229–242.

40. Greenspan, L. 1977. Humidity fixed points of binary saturated aqueous solutions. *J. Res. Natl. Bur. Stand.* 81A:89–95.

41. Barth, A. 2007. Infrared spectroscopy of proteins. *Biochim. Biophys. Acta.* 1767:1073–1101.

42. Susi, H., and D. M. Byler. 1983. Protein structure by Fourier transform infrared spectroscopy: second derivative spectra. *Biochem. Biophys. Res. Commun.* 115:391–397.

43. Leekumjorn, S., and A. K. Sum. 2007. Molecular characterization of gel and liquid-crystalline structures of fully hydrated POPC and POPE bilayers. *J. Phys. Chem. B.* 111:6026–6033.

44. Kučerka, N., M.-P. Nieh, and J. Katsaras. 2011. Fluid phase lipid areas and bilayer thicknesses of commonly used phosphatidylcholines as a function of temperature. *Biochim. Biophys. Acta.* 1808:2761–2771.

45. Venable, R. M., H. I. Ingólfsson, …, R. W. Pastor. 2017. Lipid and peptide diffusion in bilayers: the Saffman-Delbrück model and periodic boundary conditions. *J. Phys. Chem. B.* 121:3443–3457.

46. Sarcina, M., N. Murata, …, C. W. Mullineaux. 2003. Lipid diffusion in the thylakoid membranes of the cyanobacterium *Synechococcus* sp.: effect of fatty acid desaturation. *FEBS Lett.* 553:295–298.

47. Vermeer, L. S., B. L. de Groot, ..., J. Czaplicki. 2007. Acyl chain order parameter profiles in phospholipid bilayers: computation from molecular dynamics simulations and comparison with ^{2}H NMR experiments. *Eur. Biophys. J.* 36:919–931.

48. Bratt, P. J., and L. Kevan. 1993. Electron spin resonance line-shape analysis of x-doxylstearic acid spin probes in dihexadecyl phosphate vesicles and effect of cholesterol addition. *J. Phys. Chem.* 97:7371–7374.

49. Ferreira, T. M., F. Coreta-Gomes, ..., D. Topgaard. 2013. Cholesterol and POPC segmental order parameters in lipid membranes: solid state ^{1}H-^{13}C NMR and MD simulation studies. *Phys. Chem. Chem. Phys.* 15:1976–1989.

50. Dill, K. A., and P. J. Flory. 1980. Interphases of chain molecules: monolayers and lipid bilayer membranes. *Proc. Natl. Acad. Sci. USA.* 77:3115–3119.

51. Gu, R. X., H. I. Ingólfsson, ..., D. P. Tieleman. 2017. Ganglioside-lipid and ganglioside-protein interactions revealed by coarse-grained and atomistic molecular dynamics simulations. *J. Phys. Chem. B.* 121:3262–3275.

52. Tomczak, M. M., D. K. Hincha, ..., J. H. Crowe. 2002. A mechanism for stabilization of membranes at low temperatures by an antifreeze protein. *Biophys. J.* 82:874–881.

53. Popova, A. V., and D. K. Hincha. 2003. Intermolecular interactions in dry and rehydrated pure and mixed bilayers of phosphatidylcholine and digalactosyldiacylglycerol: a Fourier transform infrared spectroscopy study. *Biophys. J.* 85:1682–1690.

54. Popova, A. V., and D. K. Hincha. 2011. Thermotropic phase behavior and headgroup interactions of the nonbilayer lipids phosphatidylethanolamine and monogalactosyldiacylglycerol in the dry state. *BMC Biophys.* 4:11.

55. Kapla, J., B. Stevensson, ..., A. Maliniak. 2012. Molecular dynamics simulations of membranes composed of glycolipids and phospholipids. *J. Phys. Chem. B.* 116:244–252.

56. Castro, V., S. V. Dvinskikh, ..., A. Maliniak. 2007. NMR studies of membranes composed of glycolipids and phospholipids. *Biochim. Biophys. Acta.* 1768:2432–2437.

57. Pluhackova, K., T. A. Wassenaar, ..., R. A. Böckmann. 2015. Spontaneous adsorption of coiled-coil model peptides K and E to a mixed lipid bilayer. *J. Phys. Chem. B.* 119:4396–4408.

58. Chandra, S., X. Chen, ..., T. C. Südhof. 2003. A broken alpha-helix in folded alpha-synuclein. *J. Biol. Chem.* 278:15313–15318.

59. Davidson, W. S., A. Jonas, ..., J. M. George. 1998. Stabilization of alpha-synuclein secondary structure upon binding to synthetic membranes. *J. Biol. Chem.* 273:9443–9449.

60. Eliezer, D., E. Kutluay, ..., G. Browne. 2001. Conformational properties of alpha-synuclein in its free and lipid-associated states. *J. Mol. Biol.* 307:1061–1073.

61. Hundertmark, M., R. Dimova, ..., D. K. Hincha. 2011. The intrinsically disordered late embryogenesis abundant protein LEA18 from Arabidopsis thaliana modulates membrane stability through binding and folding. *Biochim. Biophys. Acta.* 1808:446–453.

62. Pinot, M., S. Vanni, ..., H. Barelli. 2014. Lipid cell biology. Polyunsaturated phospholipids facilitate membrane deformation and fission by endocytic proteins. *Science.* 345:693–697.

63. Garten, M., C. Prévost, ..., S. Vanni. 2015. Methyl-branched lipids promote the membrane adsorption of α-synuclein by enhancing shallow lipid-packing defects. *Phys. Chem. Chem. Phys.* 17:15589–15597.

64. Strandberg, E., D. Tiltak, ..., A. S. Ulrich. 2012. Lipid shape is a key factor for membrane interactions of amphipathic helical peptides. *Biochim. Biophys. Acta.* 1818:1764–1776.

65. Vamparys, L., R. Gautier, ..., P. F. Fuchs. 2013. Conical lipids in flat bilayers induce packing defects similar to that induced by positive curvature. *Biophys. J.* 104:585–593.

66. Koller, D., and K. Lohner. 2014. The role of spontaneous lipid curvature in the interaction of interfacially active peptides with membranes. *Biochim. Biophys. Acta.* 1838:2250–2259.

67. Artus, N. N., M. Uemura, ..., M. F. Thomashow. 1996. Constitutive expression of the cold-regulated *Arabidopsis thaliana COR15a* gene affects both chloroplast and protoplast freezing tolerance. *Proc. Natl. Acad. Sci. USA.* 93:13404–13409.

68. Vats, K., K. Knutson, ..., E. D. Sheets. 2010. Peripheral protein organization and its influence on lipid diffusion in biomimetic membranes. *ACS Chem. Biol.* 5:393–403.

69. Iyer, A., N. Schilderink, ..., V. Subramaniam. 2016. Membrane-bound alpha synuclein clusters induce impaired diffusion and increased lipid packing. *Biophys. J.* 111:2440–2449.

70. Pantusa, M., B. Vad, ..., R. Bartucci. 2016. Alpha-synuclein and familial variants affect the chain order and the thermotropic phase behavior of anionic lipid vesicles. *Biochim. Biophys. Acta.* 1864:1206–1214.

71. Ramakrishnan, M., P. H. Jensen, and D. Marsh. 2003. Alpha-synuclein association with phosphatidylglycerol probed by lipid spin labels. *Biochemistry.* 42:12919–12926.

72. Thomashow, M. F. 1999. Plant cold acclimation: freezing tolerance genes and regulatory mechanisms. *Annu. Rev. Plant Physiol. Plant Mol. Biol.* 50:571–599.

73. Steponkus, P. L. 1984. Role of the plasma membrane in freezing injury and cold acclimation. *Annu. Rev. Plant Physiol.* 35:543–584.